

Eksploatacja i Niezawodnosc - Maintenance and Reliability

Volume 29 (2027), Issue 3

https://ein.org.pl

The Polish Maintenance Society

TGMM: composite fault diagnosis for aero-engine gas path using limited data

Xingchen Liu[1,*], Lingshun Liu[1], Weimin Lü[1]

[1] Naval Aviation University, China

* Corresponding Author: a1323061826@163.com

Received: 29 May 2026
Revised: 19 October 2026
Accepted: 30 October 2026
Online: 20 November 2026

This is an open access article under the CC BY 4.0 license

Abstract

Aero-engine gas path composite fault data is characterized by scarcity and imbalanced distribution, which limits existing methods from effectively mining deep feature information from raw monitoring data and further degrades the accuracy of fault diagnosis. To solve the above problem, a composite fault diagnostic method for aero-engine gas path based on Transformer Generative Adversarial Network Multiscale Mamba (TGMM) is proposed. Firstly, the Transformer Generative Adversarial Network (TransGAN) model is constructed to generate different types of fault data, which have similar feature information to the raw data and can significantly improve the accuracy of fault diagnosis. On this basis, the multiscale Mamba is designed to perform fault diagnosis on the generated data. By extracting local features and global dependencies from the raw data, the accurate identification is finally achieved. In the composite fault diagnosis experiments, precision, recall and F1-score of the proposed method can reach 98.1%, 99.3% and 98.7%, and has good robustness and high computational efficiency.

Keywords: *composite fault diagnosis, aero-engine, gas path, TGMM*

Article citation:
Liu X, Liu L, Lü W, TGMM: composite fault diagnosis for aero-engine gas path using limited data, Eksploatacja i Niezawodnosc – Maintenance and Reliability 2027: 29(3) http://doi.org/10.17531/ein/242347

Highlights

- The method exhibits superior performance under small-sample and imbalanced conditions.
- TransGAN-generated data notably enhances the diagnostic accuracy of baseline models.
- The multiscale Mamba delivers excellent diagnostic performance and strong robustness.

1. Introduction

As the main power unit of an aircraft, aero-engine has been operating under prolonged harsh conditions, which can lead to performance degradation or even malfunctions, thereby causing safety problems [1]. Among all the types of faults in aero-engines, gas path faults are one of the most important types [2], mainly including blade wear, injector clogging and nozzle corrosion [3]. Aero-engine is mainly through the gas path system to maintain the balance of the flow and pressure of the whole engine, whether the gas path system is operating normally or not directly affects the overall performance of the engine. Therefore, how to diagnose the latent gas path faults in time and take effective means to eliminate them is an important challenge facing the field of aero-engine at present.

Synthesizing the theory of fault diagnosis technology at the current stage, fault diagnosis methods are classified as the expert knowledge-based methods, model-based methods and data-driven methods [4–6]. The first method mainly combines engineering experience and theoretical knowledge to reason about fault types, and this highly experience-dependent approach lacks stability and accuracy [7]. The second method is to construct a specific mathematical model according to operating mechanism, and study the relationship between the engine fault state and the change of performance parameters through simulation, so as to accurately locate the faults [8]. This method has high requirements for model accuracy and a low degree of generalization. Therefore, both of these two methods have limitations. The data-driven method is to mine the potential fault features through models, thereby completing the

identification of fault types [9]. This method is not only less difficult in acquiring data and building models, but also has excellent performance in accuracy, stability and generalizability, especially the deep learning algorithm that has become popular at present [10]. As one of the most cutting-edge technologies, deep learning has unparalleled advantages over traditional methods in feature extraction and learning of high-dimensional data. Therefore, it has become the focus of research in the aero-engine fault diagnosis, which has been widely developed.

Literature [11] proposed a composite fault diagnosis framework based on reinforcement learning, which achieved a significant improvement in computational speed compared to other methods. Litera-ture [12] constructed a composite fault diagnosis model that incorporated the feature extractor and ad-versarial training mechanism, and verified the effectiveness of this model through experiments. Litera-ture [13] proposed an intelligent fault diagnosis method based on the SENet structure, which reduced the dependence on fault samples and still achieved effective composite fault diagnosis under variable oper-ating conditions. Literature [14] proposed a novel diagnosis model for composite fault, which accurately decoupled and identified composite faults through a multi-label classifier, and introduced an active learning methodology to obtain more accurate results by fewer samples. Literature [15] proposed an intelligent diagnosis scheme, which mainly transformed the composite fault signal into a spectral entro-py image, effectively improving the diagnosis accuracy. Literature [16] combined the LSTM network with autoencoder to achieve deep extraction of composite fault features, thereby significantly improving diagnostic accuracy. Based on the data-driven approach, literature [17] established an effective diagnosis strategy for composite fault, and proved that this strategy had higher accuracy and stronger environmen-tal adaptability through experiments. Literature [18] proposed an advanced composite fault diagnosis method. This method learned intrinsic relationships between faults and optimized the model architecture using the boundary loss function. Literature [19] constructed an effective diagnosis model for composite fault based on migration learning, and demonstrated experimentally that the model achieved deep fea-ture extraction at low labelling rates. Literature [20] proposed an augmented element learning method based on lightweight convolutions. Experimental results demonstrated that under limited data samples, this method achieved higher accuracy compared with other comparative methods.

Among the above methods, model training requires substantial fault data, and the diagnosis accu-racy of composite fault is relatively low. In reality, the probability of gas path composite fault is extreme-ly low, which results in the fault data that can be used for training is scarce and unevenly distributed. Meanwhile, the composite fault of gas path is highly dimensional and strongly coupled. The existing methods are difficult to effectively extract the deep feature information of the raw data, which will se-verely reduce the diagnosis accuracy. Therefore, a composite fault diagnostic method based on TGMM is proposed. Firstly, according to different fault types, the TransGAN model is used to generate data that is similar to the raw data, thereby increasing the data scale and achieving the decoupling of the raw data. On this basis, the multiscale Mamba is utilized to extract multiscale local features and global dependen-cies from the raw data, the accurate composite fault diagnosis is ultimately achieved. The experimental results show that precision, recall and F1-score of the proposed method can reach 98.1%, 99.3% and 98.7%. The contributions are summarized as follows:

(1) The proposed method can significantly improve the composite fault diagnosis accuracy and ro-bustness under small samples and unbalanced conditions, which is significantly better than other meth-ods.
(2) The TransGAN model for data generation is constructed. The data generated by the TransGAN maintains the distribution pattern and feature information similar to those of the raw data, and can signif-icantly improve the diagnosis accuracy, which can facilitate the simplification of diagnosis models.
(3) The multiscale Mamba model for fault diagnosis is designed. The multiscale Mamba has high diagnostic accuracy for composite faults and exhibits good robustness.

The rest is as follows. Section 2 elaborates the TransGAN model. Section 3 provides a detailed de-scription of the multiscale Mamba model. Section 4 indicates the overall process of fault diagnosis. Sec-tion 5 analyzes the experimental

results. Finally, the research findings are summarized in Section 6, and suggestions are made for future research directions.

2. TransGAN

According to different types of faults, the TransGAN model is constructed to generate high-quality fault data, thereby increasing the scale and diversity of the raw data. The generator and discriminator of the TransGAN model are mainly composed of the position encoding, transformer blocks and linear lay-ers, as shown in Fig. 1.

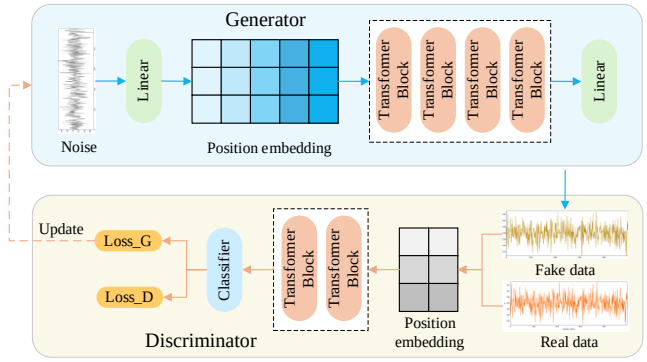

Figure 1. TransGAN model.

2.1. Position encoding

The positional encoding is generated by sine functions and cosine functions, which assign a unique encoding vector to each time step. This mechanism enables the model to effectively distinguish between elements at different locations, thus enhancing the ability to model the raw data. For odd and even dimensions, the position encoding is respectively:

$$PE_{(pos,2i)} = sin\left(\frac{pos}{10000^{\frac{2i}{d_{\text{model}}}}}\right) \quad (1)$$

$$PE_{(pos,2i+1)} = cos\left(\frac{pos}{10000^{\frac{2i}{d_{\text{model}}}}}\right) \quad (2)$$

Where pos is the position index; d_{model} is the model dimension.

2.2. Transformer block

The transformer block consists of multi-head attention, feed forward network, residual connection and layer normalization [21], among which the latter two are utilized to alleviate gradient disappearance and accelerate the training process.

2.2.1. Multi-head attention

The multi-head attention is the core computing module in the transformer architecture, as shown in Fig. 2. By running multiple independent attention heads in parallel, the multi-head attention mechanism enables the model to simultaneously extract information from different subspaces of the input sequence [22]. The calculation process is as follows:

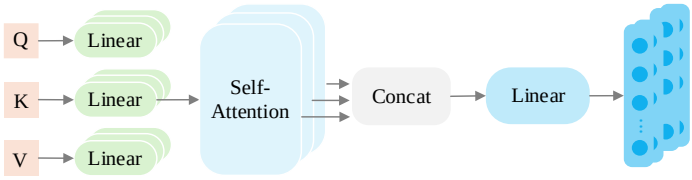

Figure 2. Multi-head attention structure.

(1) Generate query, key and value of global and individual attention heads:

$$Q = XW_Q, \quad K = XW_K, \quad V = XW_V \quad (3)$$

where X is the input feature; W_Q, W_K and W_V are the global weight matrices.

$$Q_i = QW_{Q_i}, \quad K_i = KW_{K_i}, \quad V_i = VW_{V_i} \quad (4)$$

where W_{Q_i}, W_{K_i} and W_{V_i} are the weight matrices of $i-th$ attention head.

(2) Calculate the attention weight α_i for $i-th$ attention head:

$$\alpha_i = \text{Softmax}\left(\frac{Q_i K_i^T}{\sqrt{d_k}}\right) \quad (5)$$

where $Q_i K_i^T$ is the dot product; d_k is the dimension size of the query and key in each attention head.

(3) Calculate the output of $i-th$ attention head:

$$\text{head}_i = \alpha_i V_i \quad (6)$$

(4) Perform multi-head output fusion:

$$\text{MultiHead}(Q,K,V) = \text{Concat}(\text{head}_1, \text{head}_2, \ldots, \text{head}_h)W_o \quad (7)$$

Where W_o is the output weight matrix, h is the number of attention heads.

2.2.2. Overall structure

Firstly, the position-encoded data is input into the multi-head attention module. The output and the input are summed through residual connection and layer normalization is performed. Then, the normalized features are input into a feedforward neural network, and further enhance the feature representation through two fully connected layers. Finally, the output of the feedforward neural network is again summed with the input through residual connections, and layer normalization is performed. The transformer block is shown in Fig. 3.

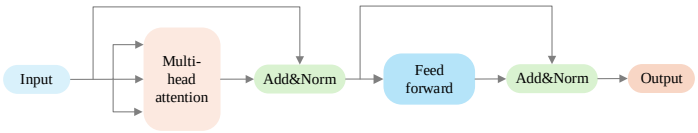

Figure 3. Transformer block.

2.3. Data generation process

The TransGAN model generates data by alternately training the generator and the discriminator. The role of the discriminator is to differentiate between real data from the raw dataset and pseudo-data from the generator to maximize its classification ability, and the goal of the generator is to make the discriminator misclassify the generated pseudo-data as real samples to maximize its deception ability [23]. Data generation is mainly divided into two stages alternately:

(1) Fix the generator and train the discriminator. First sample N potential vectors z from the noise , use the generator to generate pseudo data, then sample N real vector x from the raw data , calculate the discriminator loss and update the discriminator weights. The loss function of the discriminator is as follows:

$$Loss_D = -\frac{1}{2}\left[\frac{1}{N}\sum_{i=1}^{N} log\, D\,(x) + \frac{1}{N}\sum_{i=1}^{N} log(1 - D(G(z)))\right] \quad (8)$$

Where $G(z)$ is the pseudo data; $D(x)$ is the judgment probabilities of real data; $D(G(z))$ is the judgment probabilities of pseudo data.

(2) Fix the discriminator and train the generator. Sample N potential vector z from the noise, calculate the generator loss and update the generator weights. The loss function of the generator is as follows:

$$Loss_G = -\frac{1}{N}\sum_{i=1}^{N} log\, D\,(G(z)) \quad (9)$$

By utilizing the powerful feature extraction and sequence modeling capabilities, the TransGAN model can generate high-quality composite fault data. This method achieves the decoupling and simplification of the raw data while increasing its scale, which helps to improve the accuracy of fault diagnosis model.

3. Multiscale Mamba

After generating data through the TransGAN model, the multiscale Mamba model is adopted to conduct fault diagnosis on the generated data.

3.1. Mamba

The Mamba model is a novel computational architecture based on selective state space models, as shown in Fig. 4. Its fundamental concept involves introducing selective information processing mechanisms to efficiently capture long-range dependencies. This model excels at leveraging computational resources to rapidly process large-scale data, addressing the limitations of traditional neural network architectures when dealing with complex sequential data [24].

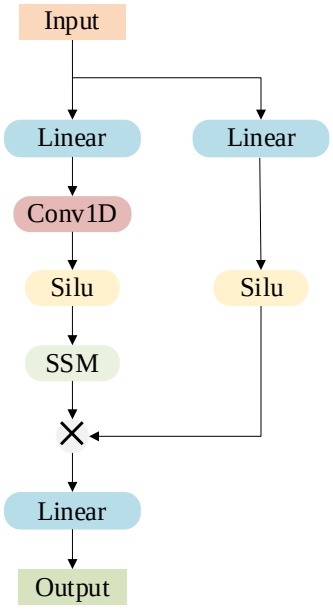

Figure 4. Mamba model.

The computational process proceeds as follows:

(1) Continuous-time state space equations:

$$h'(t) = Eh(t) + Fx(t) \quad (10)$$

$$y(t) = Hh(t) + Gx(t) \quad (11)$$

where $x(t)$, $h(t)$ $y(t)$ are respectively the input signal, hidden signal and output signal; E,F,H and G are parameter matrices.

(2) Discretization of parameter matrices:

$$\bar{E} = e^{E\Delta} \quad (12)$$

$$\bar{F} = (e^{E\Delta} - I)E^{-1}F \quad (13)$$

where Δ is the discretization step size; I is the identity matrix.

(3) Update discrete-time states:

$$h_k = \bar{E}h_{k-1} + \bar{F}x_k \quad (14)$$

$$y_k = Hh_k + Gx_k \quad (15)$$

where h_k,x_k and y_k represent the state vector, input vector, and output vector at the kth time step, respectively.

3.2. Overall structure

In order to capture the fault features at different scales within the original signal, the multiscale Mamba model is adopted to further improve the diagnosis accuracy, as shown in Fig. 5.

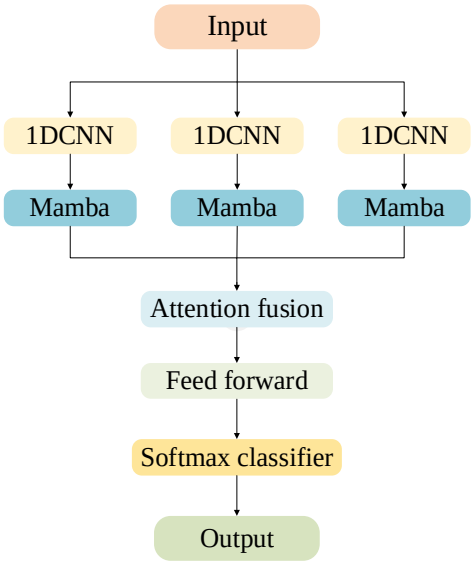

Figure 5. Multiscale Mamba model.

The whole calculation process is as follows:

(1) Calculate the output of each branch:

$$H_i = \text{ReLU}(W_i * X + b_i) \tag{16}$$

where X is the input data; W_i and b_i are respectively the weights and biases of the $i-th$ branch.

$$Y_i = \text{MambaBlock}(H_i) \tag{17}$$

(2) Calculate the attention fusion output of all branches:

$$Y = [Y_1, Y_2, Y_3] \tag{18}$$

$$Q = YW_Q, K = YW_K, V = YW_V \tag{19}$$

where Q, K and V are query, key and value; W_Q, W_K and W_V are the weight matrix.

$$Attention = \text{softmax}\left(\frac{QK^T}{\sqrt{d_k}}\right)V \tag{20}$$

where QK^T is the dot product; d_k is the dimension size of query and key.

$$Y_{attention} = \text{LayerNorm}(Attention.W_O + Y) \tag{21}$$

where W_O is the output weight matrix.

(3) Calculate the final output:

$$Y_{final} = (\text{GELU}(Y_{attention} \cdot W_1 + b_1)).W_2 + b_2 \tag{22}$$

where W_1 and W_2 are the weight matrix; b_1 and b_2 are the bias.

4. Overall process of fault diagnosis

According to different fault types, the TransGAN is firstly utilized to generate data similar to the raw data, addressing the challenges the challenges of small samples and unbalanced distributions while simultaneously achieving the decoupling and simplification of the raw data. On this basis, the multiscale Mamba is used to process the generated data. By deeply mining and extracting multiscale local features and global dependencies from the raw data, the accurate composite fault diagnosis is ultimately achieved. The overall process is shown as Fig. 6.

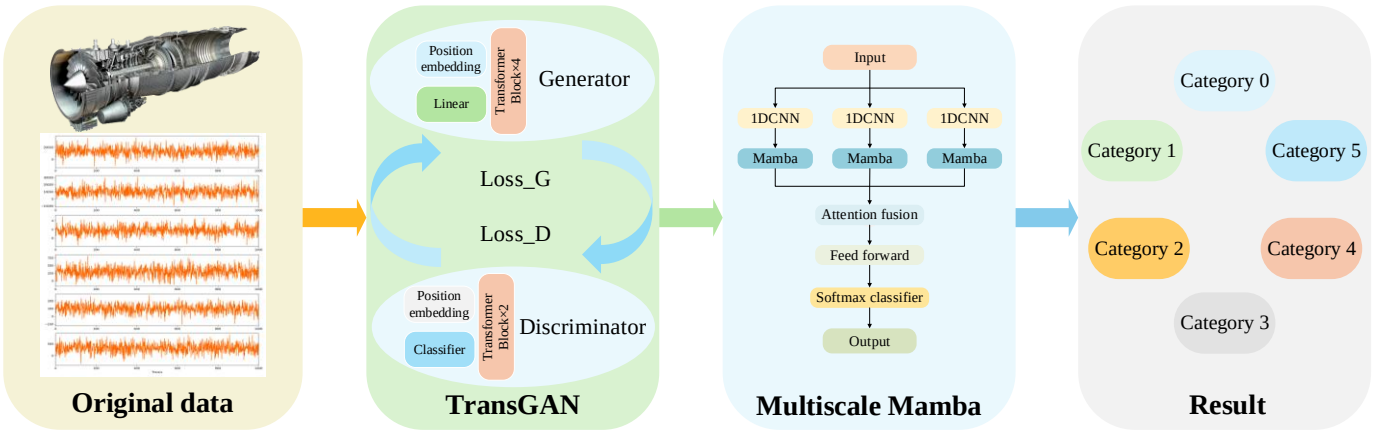

Figure 6. The overall process of fault diagnosis.

5. Experimental results and analysis

5.1. Dataset

The experiments adopt the actual operation data of an aero-engine, which are as shown in Table 1.

The dataset includes various single fault types and composite fault types, as shown in Table 2. To eliminate the influence among different feature scales, it is necessary to standardize the raw data before the experiment. The formula is specified as follows:

$$X_{norm} = \frac{X - X_{min}}{X_{max} - X_{min}} \tag{23}$$

Table 1. Parameter information of the dataset.

Number	Parameter	Units
1	High-pressure rotor speed	RPM
2	Low-pressure rotor speed	RPM
3	Total fuel flow	Kg/s
4	Total intake pressure	kPa
5	Total air intake temperature	K
6	Low-Pressure Turbine outlet pressure	kPa
7	Low-Pressure Turbine outlet temperature	K
8	High-Pressure Turbine outlet pressure	kPa
9	High-Pressure Turbine outlet temperature	K
10	High-Pressure Compressor intake pressure	kPa
11	High-Pressure Compressor outlet temperature	K
12	High-Pressure Compressor outlet pressure	kPa

Table 2. Fault settings of the dataset.

Location	Fault type	Label
HPC	Blade wear	0
HPT	Blade corrosion	1
LPT	Blade crack	2
HPC+HPT	Blade wear, blade corrosion	3
HPT+LPT	Blade corrosion, blade crack	4
HPC+HPT+LPT	Blade wear, blade corrosion and blade crack	5

5.2. Evaluation indexes

To comprehensively evaluate the results, precision, recall, F1-score and computing time are adopted as evaluation indexes, which are helpful to reduce the influence of the unbalanced distribution, thus providing a fair and accurate performance measurement [25].

$$Precision = \frac{TP}{TP+FP} \tag{24}$$

$$Recall = \frac{TP}{TP+FN} \tag{25}$$

$$F1-score = \frac{2\times TP}{2\times TP+FP+FN} \tag{26}$$

where TP is the number of samples that belong to a certain category are correctly diagnosed as the category; FP is the number of samples that do not belong to a certain category but are incorrectly diagnosed as the category; FN is the number of samples that actually belong to a certain category but are incorrectly diagnosed as other categories.

5.3. Experimental environment

The experiments use Python 3.8, and the software configuration is Pytorch 2.4.1, CUDA 11.7, and CUDNN 8.5. To eliminate the accidental errors, all experiments are repeated independently for 10 times and calculate the average values. The hyperparameters are shown in Table 3.

Table 3. Hyperparameters of the proposed method.

Sources	Hyperparameters	Value
TransGAN	seq_len	1
	num_features	12
	num_heads	4
	Learning Rate	0.001
	Batch_size	32
	Dropout_rate	0.1
Multiscale Mamba	Conv_kernel size	5,10,15
	State space dimension	16
	Expansion factor	2
	num_layer	2
	Conv_kernel_size	3
	Learning Rate	0.005
	Batch_size	16
	Dropout_rate	0.1

5.4. Data generation and quality evaluation

5.4.1. Data generation results

According to the different fault types, the TransGAN model is used for data generation, as shown in Fig. 7. The generated data not only possesses dynamic trends similar to the raw data, but also successfully retains the time-dependent and statistical distribution characteristics of the raw data. At the same time, there are some differences between the two. These differences increase the diversity characteristics of the raw data, thereby facilitating the effective training and performance enhancement of fault diagnosis model.

5.4.2. Preliminary evaluation

To preliminarily evaluate the quality of generated data, the PCA is adopted for dimensionality reduction visualization to intuitively determine whether the generated data is similar to the raw data in terms of spatial distribution and feature relationships [26]. According to the Fig. 8, from the perspective of overall distribution, the generated data exhibit a clear external profile and a uniform internal distribution with a high degree of overlap with the raw data. Despite the presence of a small number of discrete points, these points do not significantly affect the overall similarity. This indicates that the generated data better maintain the distribution pattern and fault characteristic information similar to the raw data, and have a certain degree of usability. At the same time, the differences between them enhance the data diversity, which contributes to improving the accuracy of the fault diagnosis model.

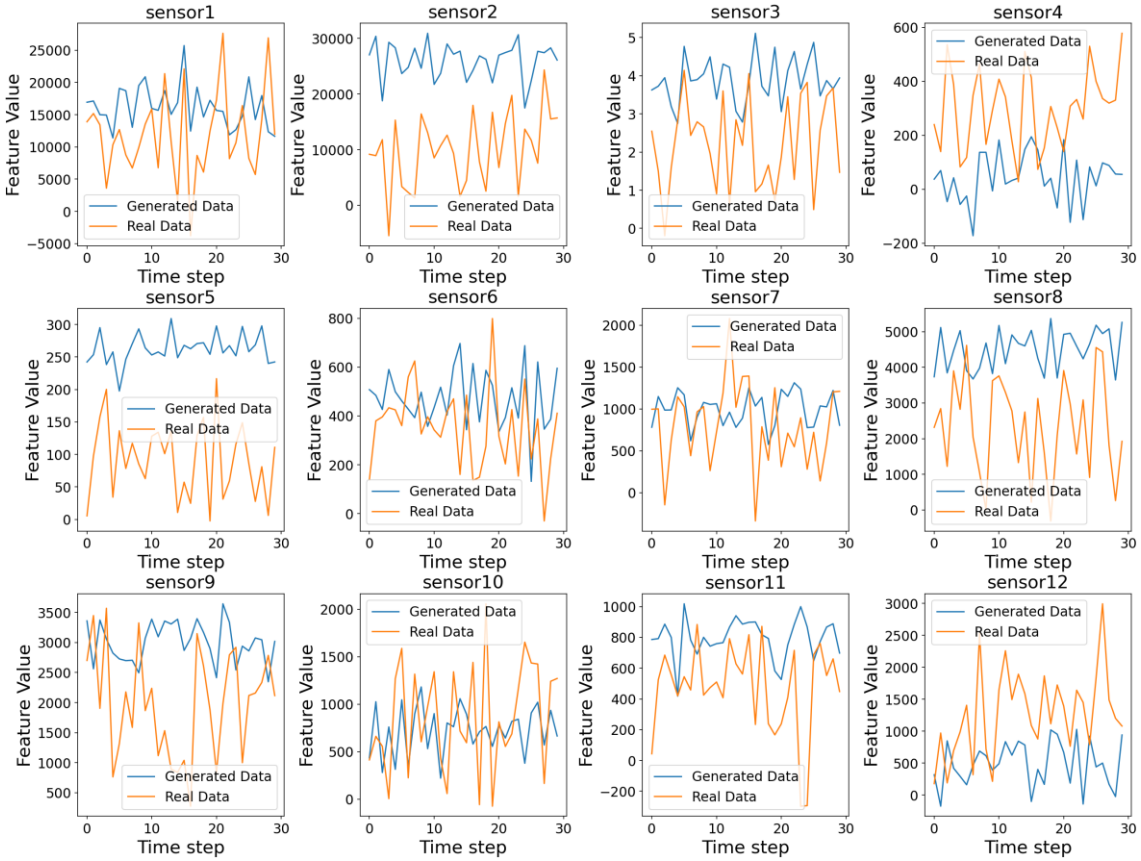

Figure 7. The result of data generation.

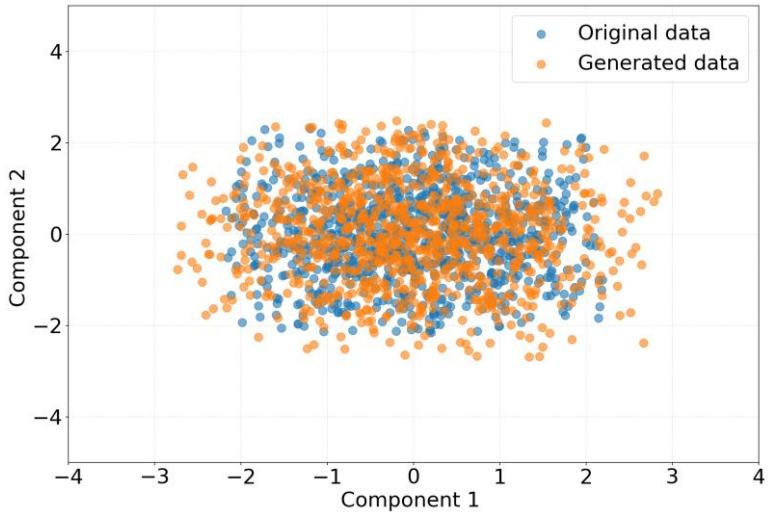

Figure 8. The visualization result of PCA.

On this basis, the Kolmogorov-Smirnov (K-S) test, Kruskal-Wallis (K-W) test and Maximum Mean Discrepancy (MMD) score are combined to further analyze the relationship between the generated data and the raw data, as shown in Table 4. Among them, the K-S test is employed to determine whether two sets of data originated from the same distribution, the K-W test is used to compare the difference in the median of the two sets of data, and the MMD score is employed to determine whether there exists a significant difference in the mean values of two data sets within a high-dimensional space. The computational formulas are respectively as follows:

$$D_{n,m} = sup\,|F_{1,n}(x) - F_{2,m}(x)| \tag{27}$$

where $F_{1,n}(x)$ is the empirical distribution functions of the raw data; $F_{2,m}(x)$ are the empirical distribution functions of the generated data. sup denotes the maximum value taken.

$$H = \frac{12}{N(N+1)} \sum_{i=1}^{k} \frac{R_i^2}{n_i} - 3(N+1) \tag{28}$$

where N is the sample size; k is the number of sample

groups; R_i is the rank sum of the first group of samples.

$$\mathrm{MMD}^2 = \frac{1}{n^2}\sum_{i,j=1}^{n} k(x_i, x_j) + \frac{1}{m^2}\sum_{i,j=1}^{m} k(y_i, y_j) - \frac{2}{nm}\sum_{i=1}^{n}\sum_{j=1}^{m} k(x_i, y_j) \quad (29)$$

where n and m are respectively the number of samples of the original and generated data; x_i and y_i are respectively the original and generated data samples; $k(x_i, x_j)$ is a kernel function.

The analysis shows that the distributions of K-S test statistic, K-W test statistic and MMD score are in the ranges of 0.25-0.42, 13.78-65.15 and 0.09-0.29, with the mean values of 0.36, 34.39 and 0.15, which are all relatively superior values. This indicates that the generated data show good similarity with the raw data both in terms of distribution patterns, statistical properties and higher order features, thereby proving that the generated data have good usability.

Table 4. Evaluation indexes for the relationship between generated data and raw data.

Label	K-S statistic	K-S p-value	K-W statistic	K-W p-value	MMD score
0	0.41	3.31e-9	21.77	0.15	0.18
1	0.32	1.43e-11	65.15	0.12	0.15
2	0.37	5.28e-10	14.73	0.24	0.09
3	0.25	3.67e-10	41.52	0.33	0.16
4	0.36	2.39e-11	49.39	0.21	0.13
5	0.42	3.02e-10	13.78	0.17	0.29

5.4.3. Qualitative evaluation

To qualitatively evaluate the quality of generated data, after mixing the raw data and the generated data in different proportions, the T-distributed Stochastic Neighbor Embedding (T-SNE) technique is used for visualization and analysis. This method is able to maintain the local structure and similarity between data points, thus making the results closer to the real state [27].

When all the data are raw data, various types of data are highly overlapping in the feature space and are difficult to distinguish. As the proportion increases, data of the same type gradually gathers to form close cluster, and the cluster spacing between different types of data gradually expands, making the whole feature space more organized. When all the data are generated, the data of each category form independent clusters in the feature space, with a high degree of differentiation between them, and only a small number of overlapping regions and discrete points exist, and the categorizable performance is significantly improved. This indicates that the data generated using the TransGAN model can not only effectively reflect the fault features in the raw data, but also show better intra-class consistency and inter-class separability, which is helpful for improving the diagnosis performance.

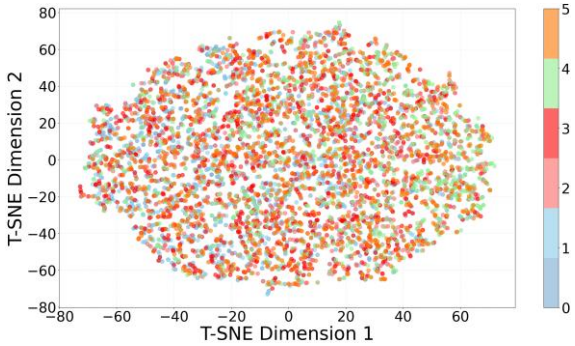

(a) Raw data

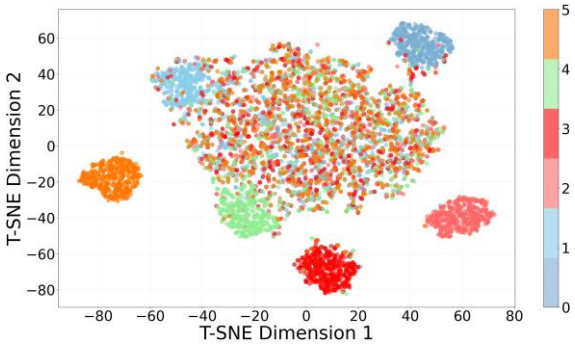

(b) The proportion is 1/3

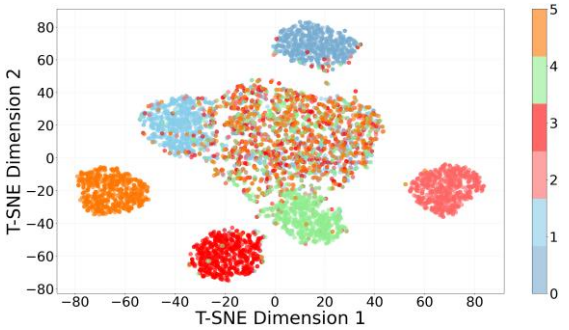

(c) The proportion is 2/3

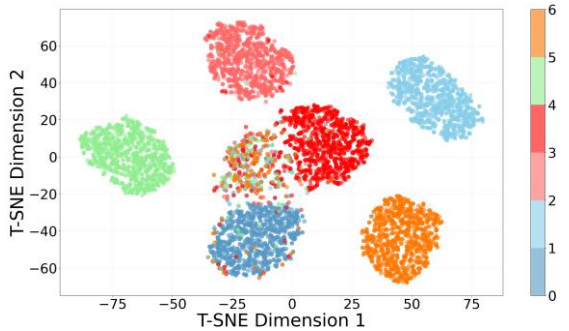

(d) Generated data

Figure 9. Visualization results of T-SNE with different proportions of generated data.

5.4.4. Quantitative evaluation

To quantitatively evaluate the data quality, experiments are conducted using three basic fault diagnosis models CNN, RNN and MLP respectively under different proportion of generated data.

Table 5. Evaluation indexes of each model in the different proportion of generated data.

Proportion	Models	Precision	Recall	F1-score	Time(s)
0%	CNN	0.119	0.114	0.116	18.56
	RNN	0.138	0.106	0.120	19.89
	MLP	0.109	0.116	0.112	20.03
1/3	CNN	0.226	0.219	0.222	18.91
	RNN	0.476	0.347	0.402	19.34
	MLP	0.388	0.281	0.326	19.63
2/3	CNN	0.536	0.382	0.446	18.78
	RNN	0.609	0.545	0.575	19.95
	MLP	0.591	0.523	0.555	20.12
100%	CNN	0.743	0.646	0.691	18.45
	RNN	0.749	0.711	0.729	20.17
	MLP	0.792	0.746	0.768	19.71

As can be seen in Table 5, when all the data are raw data, three indexes for each model are the lowest value. This is due to the fact that the raw data contains a variety of single and composite fault modes, the correlation pattern and coupling effect between the parameters are very complex, resulting in poor classifiable performance. As the proportion increases, all evaluation indexes are improved to different degrees. When the proportion is 100%, precision, recall, and F1 score of CNN, RNN, and MLP are respectively 62.4%, 53.2%, 57.5%, 61.1%, 60.5%, 60.9%, 68.3%, 63.0%, and 65.6% higher than those of the raw data. Under different proportions of generated data, the improvement in the same evaluation indexes of different models shows little variation. Additionally, the computing time differences of each model under different proportions are relatively small. Therefore, while maintaining high computational efficiency, the data generated by TransGAN can effectively improve the performance of diagnosis model and show good generalization across different models, which is helpful to the simplification of the diagnosis model.

5.5. Fault diagnosis and comparative analysis

According to the Fig. 9 (d), the distribution of generated data is clearer compared with the raw data, but there are still overlapping and discrete phenomena. This is because the composite fault features in the raw data are highly correlated and coupled, making the performance of different types of faults in the feature space extremely similar. Even after the data enhancement of TransGAN model, some faults are still not completely distinguished. At the same time, the various indexes when the proportion is 100% in the Table 5 also indicate that the use of the basic model is insufficient to achieve the optimal diagnostic effect. Therefore, more effective models are required to further enhance accuracy.

5.5.1. Fault diagnosis results

Under different generated data proportions, the multiscale Mamba model is utilized for fault diagnosis and the results are shown in Fig. 10. The diagnostic accuracy of all types of faults is improved to different degrees with the proportion increases. When all the data are generated data, the recall of the three single fault types can reach up to 100%, and even for the three composite fault types with higher degree of feature coupling, the recall can reach 98%, 99% and 98%. This indicates that the multiscale Mamba can effectively distinguish different composite fault types and achieve high classification accuracy.

5.5.2. Comparative analysis

To evaluate the diagnostic performance, the proposed method is compared with multiple advanced methods. According to the Table 6, three indexes of the proposed method are all at the highest level, which are respectively at least 2.4%, 3.9% and 3.2% higher than other methods. From the perspective of computing time, the proposed method significantly improves the accuracy with only a slight increase in time consumption, achieving a balance between model performance and computational efficiency. Therefore, the proposed method is well-suited for composite fault diagnosis and demonstrates significant advantages over other methods. Furthermore, considering Tables 5 and 6 collectively, it can be seen that both the TransGAN and the multiscale Mamba contribute significantly to the overall fault diagnosis accuracy, and both of them jointly promote the improvement of diagnostic performance.

5.6. Diagnosis experiment under different noise intensity

To compare the performance under different noise intensities, Gaussian white noise with different signal-to-noise ratios (SNRs) is added to the raw data for comparative experiments. To facilitate the comparison and analysis, the parameters of the diagnostic models remained unchanged.

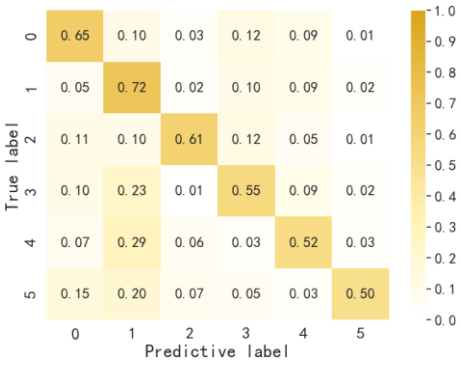

(a) Raw data

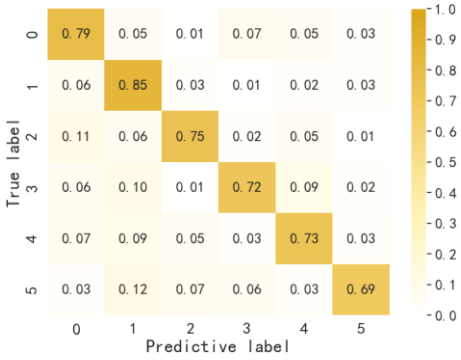

(b) The proportion is 1/3

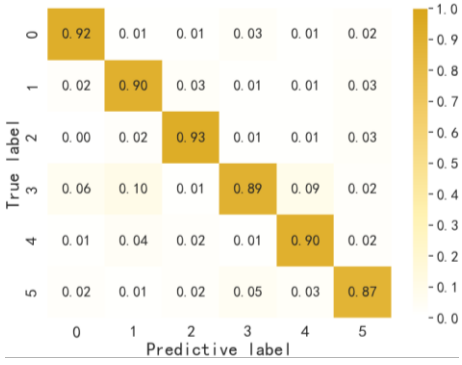

(c) The proportion is 2/3

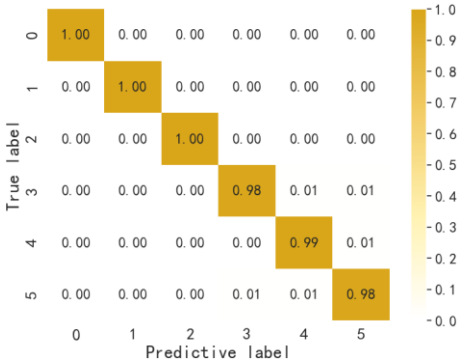

(d) Generated data

Figure 10. The results of fault diagnosis.

Table 6. Evaluation indexes of different methods.

Methods	Precision	Recall	F1-score	Time(s)
Multiscale Mamba	0.852	0.867	0.859	49.76
CDDAN [28]	0.873	0.879	0.876	56.39
SSDAE [29]	0.897	0.908	0.902	65.12
CNN-BGRU [30]	0.915	0.927	0.921	58.98
GGRU-1DCNN [31]	0.932	0.941	0.936	72.57
TL-GMVAE [32]	0.957	0.954	0.955	61.92
Proposed method	0.981	0.993	0.987	63.76

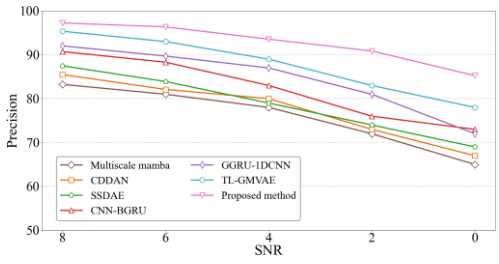

(a) Precision

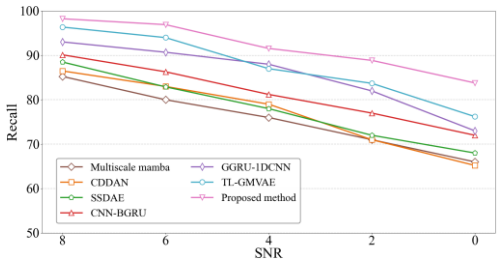

(b) Recall

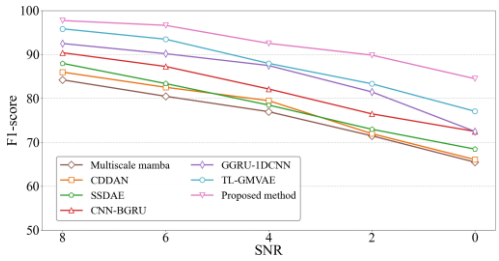

(c) F1-score

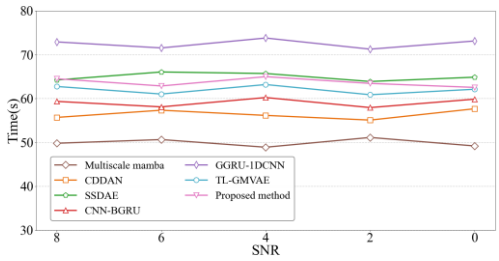

(d) Time (s)

Figure 11. Evaluation indexes of each method under different SNRs.

According to the Fig. 11, as noise intensity increases, precision, recall, and F1-score of each method decrease to varying degrees, indicating that noise exerts a certain impact on the accuracy of all models. At the extreme noise intensity of SNR0, three indexes of the proposed method are respectively improved by at least 7.25%, 7.59% and 7.42% compared with other methods. Meanwhile, the decline in each evaluation index is the smallest under different SNRs, indicating that the proposed model has good robustness. Moreover, the computational time differences of each model under different noise intensities are not significant.

6. Conclusion

The probability of gas path composite fault is extremely low, resulting in the amount of data that can be used for training is relatively scarce and unevenly distributed. Meanwhile, the gas path composite fault is highly dimensional and strongly coupled. The existing methods are difficult to effectively mine the deep feature information in the raw data, which will seriously reduce the accuracy of fault diagnosis. To solve the composite fault diagnosis problem under small samples and unbalanced conditions, a com-posite fault diagnostic method for aero-engine gas path based on TGMM is proposed. The conclusions are summarized as follows:

(1) While maintaining high computational efficiency, precision, recall and F1-score of the proposed method have increased by at least 2.4%, 3.9% and 3.2% compared with other methods. At the extreme noise intensity of SNR0, precision, recall and F1-score of the proposed method are respectively improved by at least 7.25%, 7.59% and 7.42% than other methods, and the decline in each evaluation index is the smallest under different SNRs, showing good robustness.

(2) The experimental results have confirmed that the generated data by TransGAN maintains the distribution pattern and fault characteristic information similar to that of the raw data, and can signifi-cantly improve the accuracy of basic fault diagnosis models.

(3) The precision, recall and F1-score of multiscale Mamba can reach 98.1%, 99.3% and 98.7%, which indicates that this model can effectively distinguish different composite fault types and achieve high classification accuracy.

For the composite fault diagnosis problem under small samples and unbalanced conditions, the proposed method has achieved good results, but there are still some areas for improvement: (1) The struc-ture of the model is relatively complex and has a large number of parameters. While ensuring the fault diagnosis accuracy, it is necessary to optimize the model. (2) The proposed method mainly focuses on the diagnosis of gas path composite faults, and needs to be extended to other more complex fault types in the future, so as to meet the diversified industrial needs.

References

1. Zhao J, Li Y G, Sampath S. A hierarchical structure built on physical and data-based information for intelligent aero-engine gas path diagnostics. *Applied Energy* 2023; 332: 120520. https://doi.org/10.1016/J.APENERGY.2022.120520.
2. Liao Z, Zhang R, Zhao H, Gao F, Geng J, Chen X, Song Z. Towards domain shifts: Stream fine-tuning via feed-forward fault data generation for on-board aero-engine gas-path diagnosis. *Measurement* 2024; 237: 115207. https://doi.org/10.1016/j.measurement.2024.115207.
3. Jin P, Lu F, Huang J, Kong X, Fan M. Life cycle gas path performance monitoring with control loop parameters uncertainty for aeroengine. *Aerospace Science and Technology* 2021; 115: 106775. https://doi.org/10.1016/j.ast.2021.106775.
4. Barber S, Izagirre U, Serradilla O. Best practice data sharing guidelines for wind turbine fault detection model evaluation. *Energies* 2023; 16(8): 3567. https://doi.org/10.3390/en16083567.
5. Sun X. Thermal contact conductance model of rough surfaces with inclination based on three-dimensional fractal theory. *Aircraft Engineering and Aerospace Technology* 2024; 96(2): 265-272. https://doi.org/10.1108/AEAT-02-2023-0054.
6. Li X Q, Song L K, Choy Y S. Multivariate ensembles-based hierarchical linkage strategy for system reliability evaluation of aeroengine cooling blades. *Aerospace Science and Technology* 2023; 138: 108325. https://doi.org/10.1016/j.ast.2023.108325.
7. Wang Q, Taal C, Fink O. Integrating expert knowledge with domain adaptation for unsupervised fault diagnosis. *IEEE Transactions on Instrumentation and Measurement* 2021; 71: 1-12. https://doi.org/10.1109/TIM.2021.3127654.

8. Im S H, Gu B G. Study of induction motor inter-turn fault part II: online model-based fault diagnosis method. *Energies* 2022; 15(3): 977. https://doi.org/10.3390/en15030977.
9. Wang Z, Xuyun F U, Zhang R. Knowledge and data jointly driven aeroengine gas path performance assessment method. *Chinese Journal of Aeronautics* 2024; 37(5):;533-557. https://doi.org/10.1016/j.cja.2023.09.011.
10. Zhao L, Mo C, Sun T. Aero-engine Gas‐Path Fault Diagnose Based on Multimodal Deep Neural Networks. *Wireless Communications and Mobile Computing* 2020; 2020(1): 8891595. https://doi.org/10.1155/2020/8891595.
11. Xu J, Wang Y, Wang Z. Transient gas path fault diagnosis of aero-engine based on domain adaptive offline reinforcement learning. *Aerospace Science and Technology* 2024; 155: 109701. https://doi.org/10.1016/j.ast.2024.109701.
12. Huang R, Li J, Liao Y. Deep adversarial capsule network for compound fault diagnosis of machinery toward multidomain generalization task. IEEE Transactions on Instrumentation and Measurement 2020; 70: 1-11. https://doi.org/10.1109/TIM.2020.3042300.
13. Kong X, Meng L, Su Y. Untrained compound fault diagnosis for planetary gearbox based on adaptive learning VMD and DSSECNN. *IEEE Sensors Journal* 2023; 23(11): 11838-11854. https://doi.org/10.1109/JSEN.2023.3265724.
14. Jin Y, Qin C, Huang Y. Actual bearing compound fault diagnosis based on active learning and decoupling attentional residual network. *Measurement* 2021; 173: 108500. https://doi.org/10.1016/j.measurement.2020.108500.
15. Li H, Gou L, Zheng H. Intelligent fault diagnosis of aeroengine sensors using improved pattern gradient spectrum entropy. *International Journal of Aerospace Engineering* 2021; 2021(1): 8868875. https://doi.org/10.1155/2021/8868875.
16. Zhang S, Qiu T. Semi-supervised LSTM ladder autoencoder for chemical process fault diagnosis and localization. *Chemical Engineering Science* 2022; 251: 117467. https://doi.org/10.1016/j.ces.2022.117467.
17. Shen Y, Khorasani K. Hybrid multi-mode machine learning-based fault diagnosis strategies with application to aircraft gas turbine engines. *Neural Networks* 2020; 130: 126-142. https://doi.org/10.1016/j.neunet.2020.07.001.
18. Yang G, Tao H, Du R. Compound fault diagnosis of harmonic drives using deep capsule graph convolutional network. *IEEE Transactions on Industrial Electronics* 2022; 70(4): 4186-4195. https://doi.org/10.1109/TIE.2022.3176280.
19. Kong X, Su Y, Meng L. Gearbox compound fault diagnosis method based on deep adversarial graph convolution transfer learning network under low label ratios. *Measurement Science and Technology*, 2023, 34(8): 085010. https://doi.org/10.1088/1361-6501/ACD13A.
20. Chen C, Wang T, Liu C. Lightweight convolutional transformers enhanced meta-learning for compound fault diagnosis of industrial robot. *IEEE Transactions on Instrumentation and Measurement* 2023; 72: 1-12. https://doi.org/10.1109/tim.2023.3277956.
21. Wang L, Chi J, Ding Y. Transformer fault diagnosis method based on SMOTE and NGO-GBDT. *Scientific Reports* 2024; 14(1): 7179. https://doi.org/10.1038/s41598-024-57509-w.
22. Li Z, Li L, Chen J. A multi-head attention mechanism aided hybrid network for identifying batteries' state of charge. *Energy* 2024; 286: 129504. https://doi.org/10.1016/j.energy.2023.129504.
23. Ferreira A, Li J, Pomykala K L. GAN-based generation of realistic 3D volumetric data: A systematic review and taxonomy. *Medical image analysis* 2024; 93: 103100. https://doi.org/10.1016/j.media.2024.103100.
24. Xu W, Wan Y, Zhao D. Efficient Mamba: overcoming the visual limitations of Mamba with innovative structures. *Image and Vision Computing* 2025; 161: 105569. https://doi.org/10.1016/j.imavis.2025.105569.
25. Yang X, Bai M, Liu J. Gas path fault diagnosis for gas turbine group based on deep transfer learning. *Measurement* 2021; 181: 109631. https://doi.org/10.1016/j.measurement.2021.109631.
26. Bai L, Song C, Zhou X. Assessing project portfolio risk via an enhanced GA-BPNN combined with PCA. *Engineering Applications of Artificial Intelligence* 2023; 126: 106779. https://doi.org/10.1016/j.engappai.2023.106779.
27. Allaoui M, Belhaouari S B, Hedjam R. t-SNE-PSO: Optimizing t-SNE using particle swarm optimization. *Expert Systems with Applications* 2025; 269: 126398. https://doi.org/10.1016/j.eswa.2025.126398.
28. Hu J, Chen M, Tang H. An adversarial transfer learning method based on domain distribution prediction for aero-engine fault diagnosis. *Engineering Applications of Artificial Intelligence* 2024; 133: 108287. https://doi.org/10.1016/j.engappai.2024.108287.
29. Li W. Research on deep learning-based fault diagnosis methods for aero-engine gas path. In: *IET International Conference on Aircraft Utility Systems*; Xi'an, China, 2024: 2197-2202.
30. Da T N, Thanh P N, Cho M Y. Novel cloud-AIoT fault diagnosis for industrial diesel generators based hybrid deep learning CNN-BGRU

algorithm. *Internet of Things* 2024; 26: 101164. https://doi.org/10.1016/j.iot.2024.101164.

31. Sun L, Zhu X, Xiao J. A hybrid fault diagnosis method for rolling bearings based on GGRU-1DCNN with AdaBN algorithm under multiple load conditions. *Measurement Science and Technology* 2024; 35(7): 076201. https://doi.org/10.1088/1361-6501/AD3669.
32. Wang K, He A, Liu Y. Gas Path Fault Diagnosis Method Under Small Samples with Interclass Imbalance. *Journal of Engineering for Gas Turbines and Power* 2025; 147(7): 071021. https://doi.org/10.1115/1.4067739.